applied optics

Direct detection of aggregates in highly turbid colloidal suspensions of polystyrene nanoparticles

J. A. Berberich,[1,4] J. P. Scaffidi,[2,5] R. N. M. Ducay,[3] N. Phillip,[3] J. T. Boivin,[1] P. T. Judge,[3] L. M. Bali,[3] and S. Bali[3,*]

[1]Department of Chemical, Paper, and Biomedical Engineering, Miami University, Oxford, Ohio 45056, USA
[2]Department of Chemistry, Miami University, Oxford, Ohio 45056, USA
[3]Department of Physics, Miami University, Oxford, Ohio 45056, USA
[4]e-mail: berberj@miamioh.edu
[5]e-mail: scaffijp@miamioh.edu
*Corresponding author: balis@miamioh.edu

Received 14 April 2015; revised 6 June 2015; accepted 23 June 2015; posted 24 June 2015 (Doc. ID 238026); published 16 July 2015

We demonstrate a total internal reflection-based method that detects, for the first time to the best of our knowledge, directly without any sample dilution or special sample preparation, the presence of aggregates in highly turbid aqueous suspensions of polystyrene nanospheres. Aggregation is induced by changing either the sample pH or ionic strength. The polystyrene mass density in our samples is two orders of magnitude higher than previously reported polystyrene aggregation studies. In cases when aggregates have formed but do not yet occupy a significant fraction of the sample volume, our sensor outperforms state of the art techniques such as dynamic light scattering in terms of sensitivity. Conversely, when the sample volume is dominated by aggregates, our sensor is not as effective.

OCIS codes: (110.0113) Imaging through turbid media; (120.2130) Ellipsometry and polarimetry; (260.6970) Total internal reflection; (280.4788) Optical sensing and sensors; (290.5820) Scattering measurements; (290.7050) Turbid media.

http://dx.doi.org/10.1364/AO.54.006461

1. INTRODUCTION

Nanoparticle aggregation—the agglomeration of nanoparticles into larger clusters—critically impacts diverse applications in bio and environmental sensing. These applications range from manipulating cellular uptake for drug delivery [1,2] and synthesizing safe nanovaccines [3,4] to enhancing the efficiency of potential cancer therapies [5] and assessing the toxicity of nanomaterials released into the environment [6]. For this reason, the detection and modeling of nanoparticle aggregation is an intensely researched topic [7].

The detection of nanoparticle aggregation in highly turbid media, directly without any sample dilution, is a challenging problem which remains relatively unexplored. Important examples of highly turbid media are biotissue [8], intravenous lipid emulsions [9], and crude petroleum [10]. The detection of unwanted nanoaggregation in intralipid emulsions [11,12] and in nanovaccines [3] that may cause thrombosis, and of asphaltene aggregates in crude petroleum that may stall oil production and transportation [10], are examples of critical issues faced by researchers that remain open problems.

In a turbid colloid, the scatterer particle size is comparable to the optical wavelength. Turbidity is quantitatively defined by the attenuation coefficient (α in cm^{-1}), through Beer's Law: the intensity $I(z)$ of a light beam propagating in the z direction through the medium is given by $I(z) = I_0 \exp(-\alpha z)$, where I_0 is the intensity at $z = 0$. Scattering media with α values greater than 200 cm^{-1} are typically classified as highly turbid. Conventional transmission-based imaging methods such as microscopy and spectrophotometry, and scattering-based particle sizing techniques such as dynamic light scattering (DLS), fail for highly turbid media owing to the extreme attenuation. Invariably, sample dilution is required before transmission- and scattering-based imaging techniques may be reliably used. Further, the level of dilution must be heavy, because optical techniques are typically based on Beer's Law and/or Mie theory, both of which assume the presence of only single-scattering events [13–15]. However, in the specific context of nanoaggregation, it has been noted that dilution although commonly used may, in many situations, alter the level or extent of aggregation [10,16].

In order to determine whether aggregation has occurred or not in a highly turbid medium it is, therefore, natural to turn toward total internal reflection (TIR) based imaging methods where the sample penetration lengths are small, on the order of an optical wavelength, so that the single-scattering assumption is satisfied (i.e., $\alpha z \ll 1$ so that no multiple scattering occurs) despite the high attenuation encountered in dense colloids [17].

Among TIR-imaging methods, some of the most widely used state-of-the-art techniques are based on surface plasmon resonance (SPR) in a metal film, usually gold, deposited on a glass surface—the sample is placed on top of the gold-coated glass surface. But SPR is typically used for measuring refractive index changes via shifts in resonant absorption frequency, not for tracking changes in attenuation coefficient [18]. Furthermore, SPR is optimized for use with metallic nanoparticles, not nonplasmonic colloids which are found in biotissue [8], intralipid emulsions [12], and crude petroleum [10], or are used as drug delivery platforms [3,4]. Recently one of us proposed an alternative sensing technique based on a new empirical model for total internal reflection (TIR) in highly turbid media which does not use SPR—instead the sample is placed directly on the glass surface [19,20]. Using this new model, accurate measurement of the attenuation coefficient, refractive index, and particle size has been demonstrated in highly turbid, though unaggregated, monodisperse aqueous suspensions of polystyrene nanospheres [17] and intralipid emulsions [21].

In this paper we show that it is possible to detect aggregation using TIR in idealized highly turbid aqueous polystyrene nanosphere suspensions, directly without any sample dilution, by tracking the attenuation coefficient. For polystyrene, scattering dominates at visible wavelengths, and absorption may be neglected [22]. We show that in this case, the attenuation coefficient is a far more sensitive indicator of aggregation than the refractive index. The polystyrene mass density in our samples is two orders of magnitude higher than previously investigated in polystyrene aggregation studies [16,23]. At these high particle concentrations aggregates start forming immediately upon mixing of the aggregating agent, on a time-scale too fast for us to monitor. However, when the aggregated sample is placed on top of our TIR sensor, these aggregates slowly settle, on a time-scale of a few minutes, due to gravity. Some aggregates approach within a wavelength of the glass-sample interface, causing a detectable increase in attenuation coefficient. Varying degrees of aggregation-induced settling are produced by adding acid or salt solutions of different concentrations, and the attenuation coefficient is recorded as a function of the concentration of the aggregating agent. It is critical to demonstrate that the particle-settling observed by our sensor is directly caused by aggregation and nothing else. We do this in two ways. First, we compare the observed settling data for carboxylated versus noncarboxylated polystyrene spheres and ensure that the data are consistent with the expected aggregation behaviors. Second, we observe the size distribution of the aggregates, albeit after heavy sample dilution, using a standard particle-sizing technique such as DLS. We find that though DLS results are consistent with our sensor, DLS is not as sensitive to the presence of aggregates as our sensor. We show that our sensor works best when the aggregates are no more than two- or three- particle aggregates, but fails when much larger aggregates form. Note that for the small levels of aggregation measured in this work, while our sensor detects aggregation-induced settling in just a few tens of seconds, a visual inspection (Fig. 1) of the free-standing colloidal samples fails to distinguish between unaggregated and aggregated solutions even after several days of observation.

To the best of our knowledge, our work constitutes a first detection of small amounts of aggregation in highly dense colloidal suspensions without any sample dilution or special sample preparation. Conversely, our sensor may also be used to detect small changes in sample pH.

Our paper is organized as follows. In Section 2 we outline our sensor design and theoretical model, and elucidate aggregation-induced settling which forms the basis for our aggregate-sensing method. In Section 3 we describe how our samples are prepared and present data on aggregate detection in carboxylated versus noncarboxylated polystyrene nano spheres at low acid/salt concentrations. Next, we present results from DLS measurements which are consistent with our sensor, though our sensor outperforms DLS in sensitivity. Finally, we examine limitations of our sensor at high acid/salt concentrations. Section 4 describes the main results in our work and offers concluding remarks.

2. EXPERIMENTAL METHOD

A. Sensor Design

Our experimental setup has been described in detail earlier [17,19–21,24]. A turbid sample of refractive index $n_s = n_r + in_i$ is placed on a glass prism of known refractive index n_p. Here, n_i is related to α through the relation $\alpha = 2n_i\omega/c$, where $\omega/2\pi$ is the laser frequency and c is the speed of light. The sample is illuminated as shown in Fig. 2(a) by a spatially divergent p-polarized beam of intensity I_i from a laser diode pigtailed to a single mode fiber.

The single mode fiber ensures a clean Gaussian spatial profile. Here, the beam power incident on the prism, the center wavelength of the source, and the source spectral bandwidth are 17 μW, 653 nm, and ±4.5 nm, respectively. The light reflected from the prism-sample interface, denoted by I_r, is

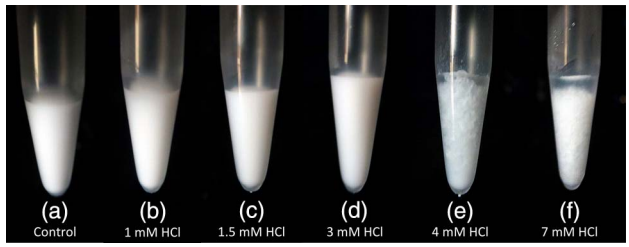

Fig. 1. Highly turbid aqueous suspension of carboxylated polystyrene spheres of nominal diameter 330 nm: (a) without aggregation; (b)–(f) with aggregation-induced settling caused by addition of varying concentrations of hydrochloric acid. All samples (a)–(f) were allowed to sit for several days before taking these photographs. Our sensor detects aggregates at acid concentrations as low as 1.25 millimolar (mM), long before large sedimented flocs and a clear top-layer become visible to the unaided eye at 4 mM HCl and higher.

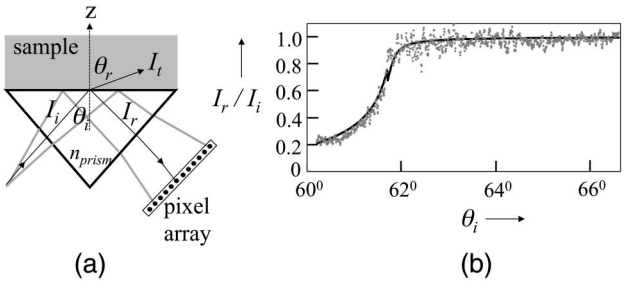

Fig. 2. (a) Prism-sample interface. Gravity points downward in the $-z$ direction; (b) plot of reflectance profile $I_r/I_i(\theta_i)$ for a highly turbid sample in which aggregation was induced by adding a 1.5 mM HCl solution.

allowed to fall on a one-dimensional pixel array (1024 pixels, each of width 14 μm), and the intensity in each pixel is read out in near-real-time using a *LabVIEW* program. The sample volume is ∼0.3 ml, sufficient to cover the laser spot size (∼3–4 mm) at the prism-sample interface. The central portion of this laser spot, ∼1.5 mm, is imaged onto the pixel array. The range of angles θ_i incident on the prism-sample interface that are detected by the pixel array spans both TIR and non-TIR regions, yielding a reflectance profile $I_r/I_i(\theta_i)$ as shown in Fig. 2(b). First, we measure the reflected intensity profile with no sample (this yields $I_i(\theta_i)$ provided TIR occurs at the prism-air interface for all θ_i). The measurement is repeated 100 times, and an average profile is generated—this process takes 10 s. Next, the sample is placed on the prism, and the average reflected intensity profile is similarly generated, yielding $I_r(\theta_i)$. Finally, the ratio of the two profiles is taken, yielding $I_r/I_i(\theta_i)$, for which each datapoint in Fig. 2(b) is represented by a gray dot. The error bar on each datapoint is smaller than the dot size.

B. Theoretical Model

The solid line in Fig. 2(b) is a theoretical fit derived from our empirical model for TIR from highly turbid media, described previously in Refs. [17,19,20]. In TIR there is angle-dependent penetration into the sample of the incident light, and the penetration depth of the evanescent wave (which is on the scale of an optical wavelength λ) in transparent samples is well-known [25]. However, in the case of a highly turbid medium there is detectable loss in TIR intensity owing to scattering even for these small penetration depths, which had not been carefully accounted for until our work in Refs. [17,19,20], and recent elegant work by others [26–28]. Our model calculates the scattering-induced loss in TIR intensity by introducing the concept of an angle-dependent n_i, i.e., $n_i(\theta_i) = n_i\kappa(\theta_i)$. In the non-TIR regime, n_i is a constant, and κ is unity for all angles, in which case we revert to traditional Fresnel theory. But in the TIR regime κ is given by [19,20]

$$\kappa(\theta_i) = \left(4\pi n_{\text{prism}}\sqrt{(M-L)/2}\right)^{-1}, \quad (1)$$

where $L=[(n_r^2-n_i^2)/n_{\text{prism}}^2]-\sin^2\theta_i$, $M=\sqrt{P^2-2L\sin^2\theta_i-\sin^4\theta_i}$, and $P = (n_r^2 + n_i^2)/n_{\text{prism}}^2$ [19,20]. In Eq. (1), κ is the ratio of the penetration depth to the optical wavelength. The angle-dependent penetration depth of an evanescent wave in TIR is well known in transparent media. Equation (1) gives the corresponding expression in a colloidal medium.

Our sensing approach is to measure the angular reflectance profile $I_r/I_i(\theta_i)$, and fit the data using the Fresnel reflectance formula

$$\frac{I_r}{I_i}(n_r, n_i, \theta_i) = \frac{M + P^2\cos^2\theta_i - \sqrt{2}\cos\theta_i(M+\sin^2\theta_i)\sqrt{M+L}}{M + P^2\cos^2\theta_i + \sqrt{2}\cos\theta_i(M+\sin^2\theta_i)\sqrt{M+L}}, \quad (2)$$

but with the angle-dependent n_i in Eq. (1) that we constructed from our model, not the constant n_i used in traditional Fresnel theory. Note that the angle-dependent n_i in Eq. (1) is written in terms of M and L that themselves depend on n_i. We therefore start with a constant-value best guess for n_r and n_i in the expressions for L, M, and P, then construct an angle-dependent $n_i(\theta_i)$ from Eq. (1). Next, we substitute this new $n_i(\theta_i)$ into the Fresnel reflectance formula in Eq. (2) and perform a best-fit of I_r/I_i to the data by minimizing the mean-square deviation: the only two fitting parameters employed are the first best-guess values used for n_r and n_i. In a few iterations, we obtain the best possible fit yielding our final n_r and n_i (or α) values. The fit in the TIR regime where n_i is angle-dependent does not smoothly match with the fit in the non-TIR regime where n_i is constant, leading to a spike in the theoretical fit function as is seen in Fig. 2(b)—however, as explained in Ref. [17], the fit obtained to the measured reflectance profile is unprecedentedly accurate. Using our model, we recently demonstrated accurate measurement of the complex refractive index of highly turbid unaggregated aqueous suspensions of polystyrene nanospheres without any sample dilution or other form of prior sample preparation [17]. Here, we use the fit provided by our model to extract n_i and hence α. If we insist on using traditional Fresnel theory instead of our model [i.e., using a constant n_i in Eq. (2) in the TIR regime] we may still be able to obtain reasonable fits to the reflectance data, but the α-values extracted may be incorrect by factors of two or more.

From the point of view of sensing aggregation, we argue in Section 2.C that α may be a far more sensitive indicator of nanoaggregation than n_r, and present supporting evidence in Section 3.B. Our sensor permits us to directly track changes in the attenuation coefficient α as aggregation occurs in the colloidal medium.

C. Aggregation-Induced Settling—A Simple Picture

The occurrence of aggregation-induced settling causes changes in the measured reflectance profile, which leads to a change in the attenuation α extracted by our model. The sensing volume of our TIR-based sensor consists of a layer approximately λ high, just above the prism. In the simplest approximation, if we imagine the sample to be divided into vertical layers, each of height λ, particles that descend during the 10 s measurement time into the sensing volume from the contiguous layer just above serve to increase the particle concentration in the sensing volume, yielding an increase in the measured α-value. For spherical particles, the settling velocity may be estimated by

$(d^2 g\Delta\rho)/18\mu$, where d is the particle diameter 0.33 μm, g is the Earth's acceleration due to gravity, $\Delta\rho$ is the density difference 0.05 g/cm^3 between the particle (polystyrene 1.05 g/cm^3) and the carrier fluid (water 1.0 g/cm^3), and μ is the viscosity of water, 1.002×10^{-2} g/cm s [29]. The values used here for $\Delta\rho$ and μ correspond to a room temperature of 20°C. For unaggregated samples, we estimate a settling velocity of about 3 nm/s [30]. The settling process lasts for a few min.

In order to measure and compare the attenuation coefficients at different acid or salt concentrations, we choose $t =$ 20 s (this is the typical time taken to add the aggregate-inducing agent and place the sample on the sensor) as the time-point for initiating the measurement of the reflectance profile shown in Fig. 2(b). By this time, sufficient settling has occurred on the sensor. During 30 s (adding in 10 s measurement time), the single nanospheres are expected to descend by approximately 90 nm, i.e., about $\lambda/7$. In other words, there is not much migration into the sensing volume from the layer above—this situation is depicted in Fig. 3(a). The possibility of particle aggregation owing to effects such as electrostatic interaction or hydrophobicity in the aqueous polystyrene suspensions has been suppressed by the manufacturer by the use of deionized water and surfactant, respectively. Thus there is significant aggregation only when specifically induced by the introduction of an acid or salt solution. When aggregation occurs, clumps of two or more particles form. The settling velocity increases as the square of the particle diameter which means we may, in a crude approximation, expect two-particle aggregates to descend at about four times the rate of a single particle, i.e., $\lambda/2$ in 30 s, and three- and four-particle aggregates are expected to fall by distances exceeding λ. Thus, in addition to aggregates that form within the sensing volume, many aggregates that form in the contiguous λ-thick layers just above fall into the sensing volume, thereby increasing the particle concentration sensed, and hence the measured attenuation α and refractive index n_r. However, more important than the concentration increase itself is the fact that this increase is caused primarily by the induction of larger particles into the sensing volume. As discussed in Section 3.B below, the larger particles scatter significantly more causing the attenuation coefficient α to have a strong dependence on particle size, far stronger than the concentration-dependence shown by both n_r and α. Therefore, in the context of nanoaggregation sensing, we expect α to be a far more sensitive indicator than n_r.

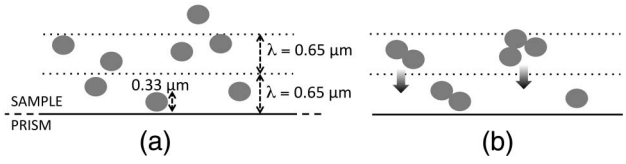

Fig. 3. (a) For an unaggregated sample, the particles displace by a small fraction of λ owing to settling, causing minimal change in the average number of particles in the sensing volume; (b) When aggregates form they fall into the sensing volume from sample layers above, increasing the particle size and concentration sensed, hence also increasing α.

3. DATA AND DISCUSSION

A. Sample Preparation

As mentioned earlier, it is critically important to prove our hypothesis that the particle settling detected by our sensor is actually aggregation-induced and not due to some other unrelated effect. We therefore choose to test our sensor on aqueous suspensions of carboxylated and uncarboxylated polystyrene nanospheres. The aggregating behaviors of carboxylated versus noncarboxylated particles offer important checkpoints for validating our hypothesis. For example, for reasons explained below in Section 3.B, small changes in pH are expected to induce aggregation in carboxylated, but not uncarboxylated, polystyrene spheres. On the other hand, small changes in ionic strength are not expected to induce aggregation in either carboxylated or noncarboxylated polystyrene spheres. However, a large change in ionic strength is expected to force aggregation in both types of spheres. All these expectations are borne out by the data shown in this section, yielding strong evidence that the settling detected by our sensor is indeed directly owing to aggregation.

We start with commercially obtained 5% w/v (or 4.76% v/v) stock solutions of carboxylated and noncarboxylated polystyrene nanospheres in deionized water [Spherotech CP-025-10 and PP-025-10, respectively]. According to the manufacturer, the carboxylated particles typically have diameter of 337 ± 66 nm, and the uncarboxylated particles have typical diameter of 266 ± 45 nm. Both types of aqueous suspensions have a pH of 7.4. The stock solutions are diluted by a factor 10 (as described in the next paragraph) for the experiments yielding a final concentration of 2.5×10^{11}/cm^3 for the carboxylated and 3.7×10^{11}/cm^3 for the uncarboxylated solutions.

We first prepare 1% w/v (0.95% v/v) aqueous polystyrene solutions by mixing four parts deionized water with one part commercial stock. Next we prepare acid (HCl) or salt (NaCl) solutions of varying concentrations. Aggregation owing to changes in pH is investigated by adding HCl solution to the polystyrene suspension. Aggregation induced by changes in ionic strength is investigated by adding NaCl solution to the polystyrene sample. Aggregation is initiated by mixing together equal volumes of a solution of the polystyrene nanospheres suspended in deionized water at twice the desired final nanosphere concentration and another solution containing the acid (HCl) or salt (NaCl) at twice the desired final acid/salt concentration. This procedure minimizes unwanted gradients in the concentration of the nanospheres and acid/salt ions at the start of the experiment [23]. For example, we mix 150 μL of 1 mM (millimolar) HCl with 150 μL of 1% w/v polystyrene solution (carboxylated or noncarboxylated) to obtain 300 μL of sample with final concentrations of 0.5 mM HCl and 0.5% w/v polystyrene. To prepare a sample with final concentration 1 mM HCl while keeping the polystyrene at 0.5% w/v, we would start with 2 mM HCl instead of 1 mM. In this way, several samples are prepared with varying HCl (or NaCl) concentration but with the same 0.5% w/v (or 0.48% v/v) polystyrene concentration.

As indicated earlier in the manuscript, our final polystyrene mass densities are two orders of magnitude higher than previously investigated in polystyrene aggregation studies

[16,23]. In Ref. [16], the diameter of the polystyrene spheres is 130 nm and the highest particle concentration employed is $5 \times 10^{10}/\text{cm}^3$, yielding a mass density of 6×10^{-5} g/cm^3. In Ref. [23], the sphere diameter is 520 nm and the highest particle concentration employed is $2 \times 10^{8}/\text{cm}^3$, yielding a mass density of 2×10^{-5} g/cm^3. By contrast, our mass density is 5×10^{-3} g/cm^3 for the carboxylated spheres and 4×10^{-3} g/cm^3 for the uncarboxylated spheres. Furthermore, given that the scattering cross section σ goes as the square of the particle radius, we may deduce that the attenuation coefficient α (which is essentially the same as the scattering coefficient $N\sigma$ in the case of polystyrene at visible wavelengths where absorption is negligible; here N is the particle concentration), and hence the turbidity, for our samples is over two orders of magnitude higher than Ref. [23] and nearly a factor 50 higher than Ref. [16].

B. Onset of Aggregation Due to Changes in pH or Ionic Strength at Low Acid/Salt Concentrations

Figure 4 shows plots of the attenuation coefficient α measured by our sensor at $t = 20$ s, for polystyrene suspensions with different concentrations of acid or salt added. In order to verify that the settling observed arises from aggregation, we compared what happens when the aggregating agent is added to an aqueous suspension of carboxylated versus uncarboxylated polystyrene spheres. Figure 4(a) shows that for carboxylated nanospheres the onset of aggregation induced by a change in pH occurs at acid concentrations as low as 1.25 mM HCl. Standard Derjaguin Landau Verwey Overbeek (DLVO) theory explains aggregation in terms of an interplay between attractive van der Waal's forces and repulsive electrostatic forces between two approaching spheres [7]. The addition of HCl causes protonation of the negative carboxyl groups by H^+ ions, resulting in the repulsive forces losing out to the attractive forces, which causes aggregation to occur. On the other hand, for noncarboxylated polystyrene spheres, aggregation dynamics are dominated by the negatively charged sulfonic groups which remain deprotonated at the pH-range used in Fig. 4(a), precluding aggregation.

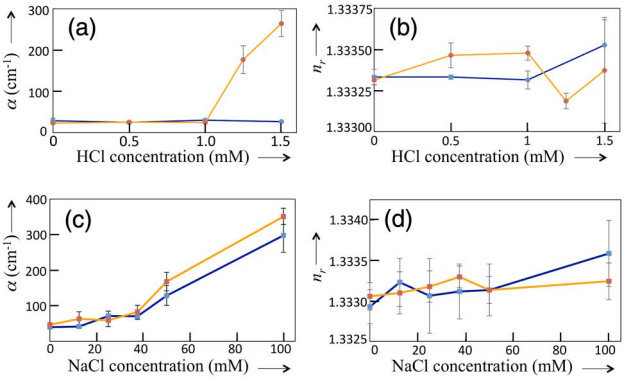

Fig. 4. Plot of: (a) α; (b) n_r for carboxylated (light orange) and noncarboxylated (dark blue) polystyrene suspensions upon addition of increasing concentrations of HCl solution (i.e., change in pH); (c) and (d) NaCl solution (i.e., change in ionic strength). pH-induced aggregation is observed for carboxylated, but not for noncarboxylated, polystyrene suspensions at low acid concentrations. Ionic strength-induced aggregation is not observed in either suspension at low salt concentration, but aggregation is forced in both suspensions at higher salt concentrations.

As the HCl concentration is increased beyond 1.5 mM, up to 2 or 2.5 mM, the attenuation coefficient α continues to rise but the theoretical fits to the reflectance data become poor and the size of the error bar increases dramatically. Reasons for this behavior, including how our sensor behaves at even higher HCl concentrations, are described in Section 3.D below.

In Fig. 4(c) we repeat the same experiment as in Fig. 4(a), but this time use NaCl as the aggregation-inducing agent. In this case, the aggregation is induced by an increase in ionic concentration of Na^+ ions (instead of protonation by H^+ ions from HCl). In both the carboxylated and noncarboxylated cases, the negatively charged sulfonic and/or carboxyl groups on neighboring polystyrene spheres are shielded from each other by the Na^+ ions in solution. At sufficient salt concentration, this charge-charge shielding can suppress repulsive interactions enough that attractive forces dominate, leading to aggregation in the simple DLVO description. Suppression of repulsive interactions between the negative charges on neighboring spheres by shielding (Na^+ ions) is a weaker effect than the near-cancellation of the negative charges by protonation (H^+ ions), therefore ionic strength-induced aggregation occurs at much higher salt concentrations than the acid concentrations required for pH-induced aggregation. Furthermore, because there are no H^+ ions to cause protonation, no significant difference in aggregating behavior is expected between the carboxylated versus the noncarboxylated polystyrene nanospheres. These expectations are borne out by our results in Fig. 4(c), proving that aggregation-induced settling may be used to sensitively detect the presence of aggregation in highly turbid colloids, without any need for sample dilution. At higher NaCl concentrations, the theoretical fits to the reflectance data become poor, as mentioned above for the HCl-polystyrene mixtures—this behavior is explained in Section 3.D below.

Figures 4(b) and 4(d) show that whereas α changes by almost an order of magnitude at the onset of aggregation, n_r changes only in the 4th decimal place and is erratic, i.e., α is a more sensitive indicator of aggregation than n_r—this is in accordance with what we stated at the end of Section 2. In order to understand the relative sensitivity of α and n_r to aggregation, we recall that aggregation-induced settling increases the particle concentration in the sensing volume and that both n_r and α are expected to vary approximately linearly with concentration. The linear concentration dependence of n_r may be seen from a straightforward examination of the usual Lorentz–Lorenz theory for homogeneous (particle size, or any sort of "granularity," does not enter this theory) nonmagnetic polarizable media [31]: for small concentrations of polystyrene spheres in water the departure of the refractive index of the solution from that of water increases linearly with the concentration of the spheres. Similarly, the explicit linear concentration dependence of α is evident from the relation $\alpha = N\sigma$ mentioned earlier in Section 3.A.

However, as pointed out in Section 2.C, far more important than any change in concentration is the fact that the aggregates settling into the sensing volume are significantly larger, comprising at least two particles. The Lorentz–Lorenz theory

ascribes no explicit dependence on particle size to n_r [31]. On the other hand, recalling that there is negligible absorption in polystyrene in the visible wavelength range and scattering dominates [22], the strong dependence on particle size of α (when particle size $\sim\lambda$) is well known in Mie scattering theory [32]. Figure 5 shows a plot of $\sigma/\pi R^2$ versus $2\pi R/\lambda'$ for an aqueous suspension of polystyrene spheres of radius R. Here λ' is the wavelength actually seen by the Mie scatterer: in our case, the polystyrene nanosphere is suspended in deionized water (refractive index 1.333), so λ' is 653/1.333, i.e., 490 nm. Note that for both carboxylated and noncarboxylated polystyrene nanospheres in our experiment, $2\pi R/\lambda' \approx 2$, placing us within the regime $2\pi R/\lambda' < 10$ in Fig. 5 where $\sigma/\pi R^2$ exhibits a single-valued increase with particle size. If we model the increase with particle size as linear in this regime, we may readily deduce that according to Mie theory α varies as the 3rd power of the particle size, much stronger than the dependence on concentration which is merely linear. Thus, in contrast to n_r, α is extremely sensitive to the induction of aggregated particles into the sensing volume.

This result seems to contradict a recent interesting experiment [34] where it is shown that α becomes increasingly insensitive to variations in particle concentration at extremely high particle concentrations, whereas n_r remains sensitive. We point out that there is no such contradiction. First, the particle concentration for the unaggregated polystyrene solution used in our work (0.48% v/v) is nearly a factor 50 less than the maximum concentration (20.9% v/v) used in Ref. [34] (the particle sizes are about the same in both works). From Fig. 8 in Ref. [34] we see that α shows no decrease in sensitivity until the concentration is nearly an order of magnitude higher than the particle concentration used in our experiment. Second, it may seem that once aggregates form in our experiment and our sample turbidity becomes comparable to Ref. [34], the conclusion from Ref. [34] may apply to our experiment, but this is not true because of the very different mechanisms by which the sample turbidity increases in Ref. [34] and our experiment. In Ref. [34] the increase in imaginary refractive index (and hence α) is caused only by an increase in particle concentration. By contrast, the mechanism behind α-increase in our experiment is aggregation, i.e., the induction of aggregates significantly larger in size than the original monomers into our sensor's sensing volume. As discussed in the previous paragraph, in our experiments, α is far more sensitive to change in particle size than change in concentration.

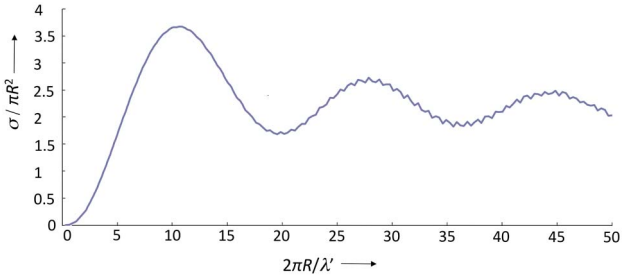

Fig. 5. Plot of Mie scattering cross section versus particle size for a polystyrene particle of n_r 1.59 [33] in deionized water illuminated by $\lambda = 653$ nm. Note that the wavelength λ' seen by the scatterer is 653 nm divided by the refractive index 1.333 of deionized water. Reference [32] shows a qualitatively similar plot for a dielectric scatterer in air of refractive index 1.33.

C. Comparison with Dynamic Light Scattering (DLS)

Besides studying the aggregation behaviors of carboxylated and noncarboxylated polystyrene spheres, another way to verify that the particle settling detected by our sensor is indeed caused by aggregation is to observe the size distribution of the aggregates using a standard particle-sizing technique such as dynamic light scattering (DLS). As is well known, DLS requires heavy dilution in the case of highly dense samples, in order to ensure that the single-scattering assumption is satisfied. During the dilution process of the polystyrene-aggregating agent mixture the sample has to be made homogeneous by stirring gently so that the polystyrene does not appear localized in one location. Care must be taken to not damage any aggregates while stirring.

Figures 6(a)–6(d) show our results, obtained using DLS to measure the size distribution in carboxylated polystyrene nano sphere solutions that have been mixed with five different solutions of HCl which range from 1 mM to 2.5 mM—in each case, the volume fraction of particles is plotted versus particle diameter. In all the DLS data here, four identical samples were prepared independently, and volume fractions for all the sizes measured in these four trials were combined and renormalized. The pair of vertical dashed lines on each plot indicates the entire range of particle sizes measured when a 1 mM HCl solution was mixed with the polystyrene solution—we measured this range to be 283–313 nm with a weighted mean of 296 nm and a standard deviation of ±10 nm. It is clear that as the HCl concentration increases from Figs. 6(a)–6(d), particles of sizes larger than 313 nm are increasingly detected. This is further illustrated in Fig. 7(a) which plots the volume fraction of particles larger than 313 nm, i.e., larger than the original size

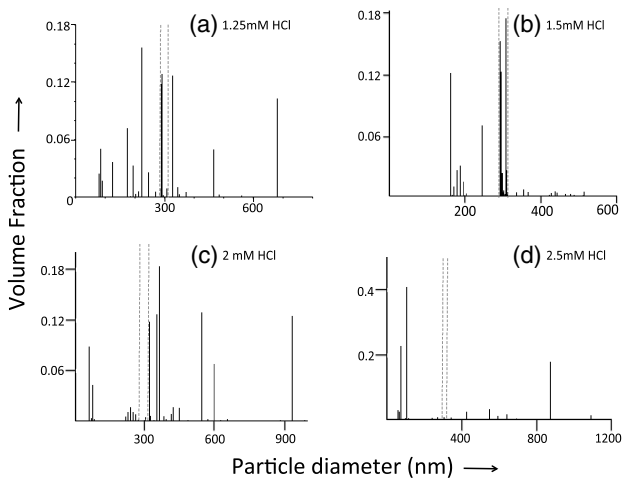

Fig. 6. Dynamic Light Scattering (DLS) results for pH-induced aggregation in suspensions of carboxylated polystyrene nanospheres mixed with five different acid concentrations. The pair of vertical dashed lines on each plot indicates the entire range of particle sizes measured when a 1 mM HCl solution was mixed with the polystyrene solution. Aggregates are observed at HCl concentrations of 2 mM and above [note the changed vertical scale for (d)], but results for 1.25 and 1.5 mM are inconclusive.

range, as a function of increasing HCl concentration from 1 to 4 mM.

Though consistent with the results from our sensor [see Fig. 4(a)], DLS is clearly outperformed in sensitivity by our sensor in the range of HCl concentrations 1–1.5 mM where the aggregates first form. Neither our sensor nor DLS detects any aggregates for the mixture of 1 mM HCl with the polystyrene suspension: Our sensor measures the same attenuation coefficient (25 cm^{-1}) for the 1 mM HCl-polystyrene mixture as for the polystyrene solution alone. However, our sensor records significant aggregation upon addition of the 1.25 mM HCl solution—the attenuation coefficient increases by a factor of 7, from 25 cm^{-1} for the polystyrene suspension alone, to 177 cm^{-1} in Fig. 4(a). At 1.5 mM HCl concentration, α is observed by our sensor to jump by over an order of magnitude from 25 cm^{-1} for the polystyrene suspension alone, to 265 cm^{-1}. By contrast, DLS claims that 30% of the sample volume is occupied by particles larger than 313 nm upon addition of 1.25 mM HCl to the polystyrene suspension, but hardly registers any aggregates at 1.5 mM HCl concentration.

We compared our sensor to DLS for the case of ionic-strength induced aggregation as well. Figures 8(a)–8(d) show results obtained using DLS to measure the size distribution of polystyrene nano spheres mixed with five different NaCl concentrations which range from 12.5 to 175 mM—again, the volume fraction of particles is plotted versus particle diameter. From the data in Fig. 4(c) and accompanying discussion we do not expect any difference in ionic strength-induced aggregating behavior between carboxylated and noncarboxylated polystyrene spheres. The data in Fig. 8 happens to be for noncarboxylated spheres. The pair of vertical dashed lines on each plot indicates the entire range of particle sizes measured when a 12.5 mM NaCl solution was mixed with the polystyrene solution—we measured this range to be 269–278 nm with a weighted mean of 274 nm and a standard deviation of ±2 nm. Just as in the case of pH-induced aggregation it is clear that as the NaCl concentration increases from Figs. 8(a)–8(d), the trend in DLS data is that particles of sizes larger than 278 nm are increasingly detected. This is further illustrated in Fig. 7(b) which plots the volume fraction of particles larger than 278 nm, i.e., larger than the original size distribution, as a function of increasing NaCl concentration from 12.5–175 mM.

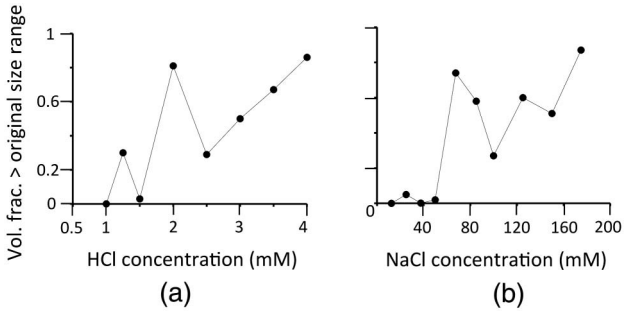

Fig. 7. Volume fraction occupied by particles larger than: (a) 313 nm in the case of HCl-polystyrene solutions; (b) 278 nm in the case of NaCl-polystyrene solutions (see text for explanation), extracted from the DLS data in Figs. 6 and 8, plotted versus the concentration of the aggregation-inducing agent. This further illustrates the trend that the number of larger particles rises with increasing HCl or NaCl concentration.

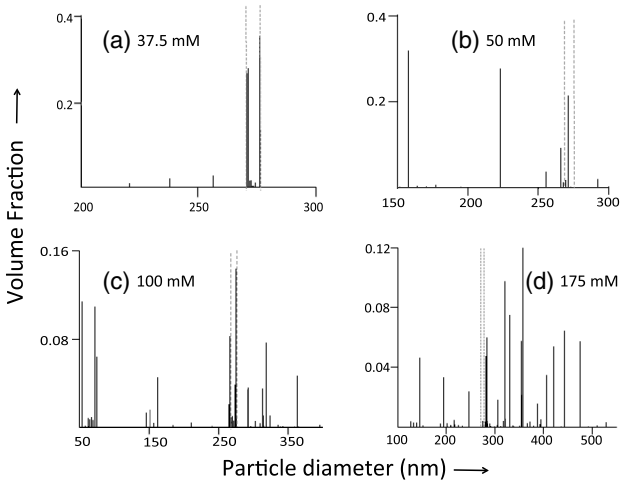

Fig. 8. Dynamic Light Scattering (DLS) results for ionic strength-induced aggregation in suspensions of noncarboxylated polystyrene nanospheres mixed with five different acid concentrations. The pair of vertical dashed lines on each plot indicates the entire range of particle sizes measured when a 12.5 mM NaCl solution was mixed with the polystyrene solution. Aggregates are observed at HCl concentrations of 100 and 175 mM, but results for 37.5 and 50 mM are inconclusive.

Just as in the case of pH-induced aggregation we again find that though consistent with the results from our sensor [see Fig. 4(c)], DLS is outperformed in sensitivity by our sensor at 50 mM NaCl concentration where the aggregates first begin to form. Our sensor records a factor 3 increase in α, from 40 cm^{-1} for the polystyrene suspension alone, to 128 cm^{-1} at 50 mM. By contrast, DLS hardly registers any aggregates at 50 mM NaCl concentration as seen in Fig. 7(b).

To summarize this section, DLS shows that aggregates form at the same concentrations of aggregation-inducing agent at which enhanced settling is observed by our sensor, providing evidence that it is indeed aggregation that is directly responsible for the settling observed by our sensor. However DLS appears to lack in sensitivity compared to our sensor at the lowest acid/salt concentrations where aggregates do not yet occupy a significant fraction of the sample volume.

D. Aggregation Behavior at High Acid/Salt Concentrations

As the concentration of aggregation-inducing agent is increased past 1.5 mM for HCl and 100 mM for NaCl, it is no longer possible to obtain from our model a good theoretical fit to the measured reflectance profile, and the value extracted for α starts exhibiting large variability. Figure 1(e), which is a photograph of the aggregated sample for the case of 4 mM HCl, suggests that this is because high acid/salt concentrations cause the formation of large flocs. The flocs in Fig. 1(e) are large enough to be readily visible to the naked eye, but it is logical to assume that samples at intermediate concentrations between 1.5 mM and 4 mM HCl [see Fig. 1(d)] also contain such multiple-particle flocs, just not large enough to be visible to the unaided

eye. For example, when a drop of the sample corresponding to, say 2 mM HCl, is deposited on top of the sensor prism, these flocs settle and accumulate in the sensor's sensing volume forming irregular macroscopic patterns approaching mm-length-scales comparable to the laser beam spot incident on the prism-sample interface. The fit to data obtained from any one sample becomes poor, as shown in Fig. 9(a), because our model assumes a homogeneous spatial distribution of scatterers distributed throughout the sensing volume, a condition that is no longer satisfied. Furthermore, the inhomogeneous spatial distribution of these flocs is different from sample-to-sample in identical data-runs on independent samples, leading to large variability in the measured values for the attenuation coefficient α. For the sample shown in Fig. 9(a) the α-value is indicated as 1193 cm^{-1}. When the measurement is repeated on five independent identical samples, the α-values extracted from fits as poor as shown in Fig. 9(a) range from 123 cm^{-1} to 1193 cm^{-1} yielding an average value $\alpha = 763$ cm^{-1} with a large error bar ± 208 cm^{-1}. Because of the poor fits and large sample-to-sample variability we do not trust the α-value extracted by our sensor for the 2 mM HCl-polystyrene samples. A similar situation occurs for the polystyrene-NaCl solutions, as seen in Fig. 9(c), for a NaCl concentration of 175 mM.

By contrast, judging from the plots in Fig. 7, at HCl concentrations beyond 2 mM and NaCl concentrations beyond 100 mM where a significant fraction of the volume is occupied by aggregates, DLS may provide a safe option to measure the extent of aggregate formation.

At even higher concentrations where the flocs are visible to the unaided eye, i.e., at 4 mM HCl and beyond [Figs. 1(e) and 1(f)], the flocs in the sample deposited on the prism surface were observed to float upward and out of the sensing volume. This causes the sample to appear clear to the sensor for the same reason that the top layer in Fig. 1(f) appears clear to the eye—the difference being that the flocs in the thin sample-layer on top of the prism spread out and float away from the prism surface, as opposed to their behavior in the radically differently shaped eppendorf tube where the flocs are unable to spread out and sink to the bottom of the tube. Figure 9(b) shows, as expected, that the measured attenuation coefficient α decreases and the theoretical fit becomes better owing to the removal of the spatially inhomogeneous flocs from the sensing volume. But the α-value extracted in this case has no meaningful information. A similar situation is observed for polystyrene-NaCl solutions, as seen in Fig. 9(d) for an NaCl concentration of 400 mM.

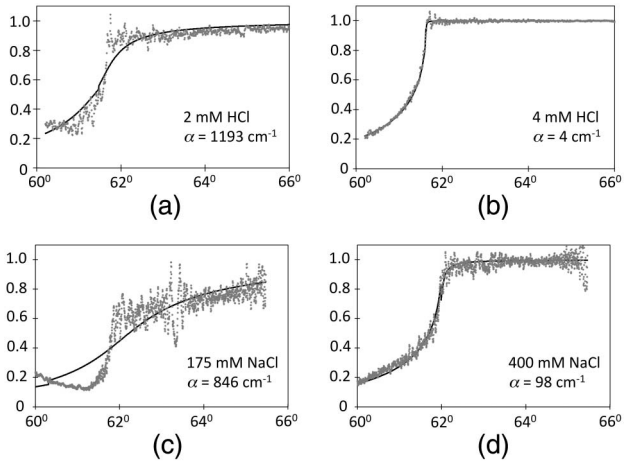

Fig. 9. These plots are reflectance profiles similar to Fig. 2(b), i.e., the x axes are the incidence angle θ_i and the y axes are I_r/I_i. Poor fits are obtained in (a) 2 mM HCl and (c) 175 mM NaCl, owing to the formation of large flocs (not yet visible to the unaided eye [see Fig. 1(d)] causing the samples to become spatially inhomogeneous. The α-values extracted by the fits in (a) and (c) are not trustworthy since the fits are poor. At even higher concentrations (b) 4 mM HCl and (d) 400 mM NaCl, the aggregated flocs are large enough to be visible to the eye [see Fig. 1(e)]. But they float upward and out of the sensing volume, causing the fits to become better, and the measured α-values to decrease. However, despite the good fits, these measured α-values provide no meaningful information on the state of aggregation since the flocs have all floated out of the sensing volume.

4. CONCLUSION

We have demonstrated a TIR-based method for sensitively detecting whether aggregates are present or not in highly turbid aqueous suspensions of polystyrene nano spheres, without the need for any dilution or special sample preparation. Aggregation is induced either by changing the pH or the ionic strength (by adding in varying concentrations of HCl, or NaCl, solutions respectively). TIR is especially suited for sensing in dense colloidal samples because the evanescent wave penetration depth is small ($\sim\lambda$) and the single-scattering assumption is satisfied (i.e., the probability for a photon to be multiply scattered is $\ll 1$), despite the sample being highly turbid. At these high particle concentrations, aggregation may occur on too fast a time-scale and directly monitoring the formation of the aggregates in real-time may not be straightforward. In our sensor we convert aggregate-detection to the simpler problem of detecting aggregation-induced settling—simpler because the time-scale for settling is much longer. Over a few minutes there is significant settling of the aggregates on to the prism of our sensor, but negligible settling of the unaggregated (lighter) particles. We developed a simple physical picture for aggregation-induced settling and confirmed in two ways that the settling we observed is indeed directly due to aggregation: First, we compared the aggregation-induced settling behaviors of carboxylated versus noncarboxylated polystyrene nano spheres. Second, we observed the size distribution of the aggregates using DLS, albeit after heavy sample dilution which is required to satisfy the single-scattering assumption on which the intensity correlation theory behind DLS is based.

Our sensor detects aggregates in the sample by directly monitoring the attenuation coefficient α in the sample volume just above the prism surface, using an empirical model of TIR in highly turbid media that we recently introduced [17,19,20]. Our model permits accurate measurement of the attenuation coefficient in highly turbid media without any sample dilution or special preparation. Based on our α-measurements and on Mie scattering arguments we have shown that, at low acid/salt concentrations, α is a far more sensitive indicator of the state of polystyrene aggregation than the real refractive index n_r. We have provided a simple explanation of the contrasting aggregation behaviors of carboxylated versus noncarboxylated

polystyrene nano spheres, using standard DLVO theory. At low acid/salt concentrations where aggregates first begin to form, our sensor not only is better than DLS in that no dilution is required but also outperforms DLS in sensitivity. On the other hand, our sensor is unable to yield size distributions like DLS.

At high acid/salt concentrations (>1.5 mM HCl, and >100 mM NaCl), where large flocs form and aggregates occupy a large fraction of the volume, our sensor is not effective but DLS is a good option (provided the heavy dilution does not pose any problem [10,16]). In the range 1.5–2 mM HCl, and 125–175 mM NaCl, the α-value measured is not trustworthy due to poor fitting by our model of the data obtained from each sample, and due to large sample-to-sample variability in the data. At higher acid/salt concentrations (>2 mM HCl, and >175 mM NaCl) the α-value measured does not provide any meaningful information on the state of aggregation due to the flocs having moved away from the sensing volume of the sensor.

In conclusion, our sensor works well for dense colloidal suspensions of polystyrene particles of size no more than about a visible optical wavelength in which some aggregates have formed but do not yet occupy a significant fraction of the volume.

We hope that our sensor's ability to sensitively monitor the state of aggregation in highly turbid media by accurate measurement of the attenuation coefficient, directly without the need for any sample dilution, will pave the way for application to sensitive noninvasive detection of nanoparticle aggregation in biological and environmentally relevant samples. Our sensor may also be used to detect small changes in sample pH in cases where injecting polystyrene nano spheres into the sample and using aggregation as a sensing tool is an option. The change in pH is only 0.1 between our polystyrene samples with 1 mM HCl (pH 3.3) and 1.25 mM HCl (pH 3.2). Our sensor may possibly find application in biological systems where minor perturbations in pH are relevant, for example, in maintaining homeostasis [35,36].

Funding. Dillon-Kane LLC; Miami University's Roundtable Interdisciplinary Fund; Petroleum Research Fund.

Acknowledgment. We thank Miami University's Instrumentation Lab for assistance in writing Labview code.

REFERENCES AND NOTES

1. K. Mohr, M. Sommer, G. Baier, S. Schottler, P. Okwieka, S. Tenzer, K. Landfester, V. Mailänder, M. Schmidt, and R. G. Meyer, "Aggregation behavior of polystyrene-nanoparticles in human blood serum and its impact on the in vivo distribution in mice," J. Nanomed. Nanotechnol. **5**, 1–10 (2014).
2. S. Akhter, I. Ahmad, M. Ahmad, F. Ramazani, and A. Singh, "Nanomedicines as cancer therapeutics: current status," Curr. Cancer Drug Targets **13**, 362–378 (2013).
3. L. Zhao, A. Seth, N. Wibowo, C. Zhao, N. Mitter, C. Yu, and A. Middelberg, "Nanoparticle vaccines," Vaccine **32**, 327–337 (2014).
4. W. De Jong and P. Borm, "Drug delivery and nanoparticles: applications and hazards," Int. J. Nanomed. **3**, 133–149 (2008).
5. Y. Yang, Y. Hu, H. Dub, and H. Wang, "Intracellular gold nanoparticle aggregation and their potential applications in photodynamic therapy," Chem. Commun. **50**, 7287–7290 (2014).
6. G. V. Lowry, K. B. Gregory, S. C. Apte, and J. R. Lead, Special issue on "Transformations of Nanoparticles in the Environment," Environ. Sci. Technol. **46**, 6891–6892 (2012).
7. W. Zhang, "Nanoparticle aggregation: principles and modeling," Adv. Exp. Med. Biol. **811**, 19–43 (2014).
8. W. Cheong, S. Prahl, and A. Welch, "A review of the optical properties of biological tissues," IEEE J. Quantum Electron. **26**, 2166–2185 (1990).
9. P. Di Ninni, F. Martelli, and G. Zaccanti, "Intralipid: towards a diffusive reference standard for optical tissue phantoms," Phys. Med. Biol. **56**, N21–N28 (2011).
10. J. Buckley, "Asphaltene deposition," Energy Fuels **26**, 4086–4090 (2012).
11. R. Michels, F. Foschum, and A. Kienle, "Optical properties of fat emulsions," Opt. Express **16**, 5907–5925 (2008).
12. D. F. Driscoll, "Lipid injectable emulsions: pharmacopeial and safety issues," Pharm. Res. **23**, 1959–1969 (2006).
13. G. D. J. Phillies, "Experimental demonstration of multiple-scattering suppression in quasi-elastic-light-scattering by homodyne cross-correlation techniques," Phys. Rev. A **24**, 1939–1943 (1981).
14. J. Dhont and C. de Kruif, "Scattered light intensity cross correlation. 1. Theory," J. Chem. Phys. **79**, 1658–1663 (1983).
15. J. Dhont and C. de Kruif, "Scattered light intensity cross correlation. 1. Experimental," J. Chem. Phys. **84**, 45–49 (1986).
16. M. Carpineti, F. Ferri, M. Giglio, E. Paganini, and U. Perini, "Salt-induced fast aggregation of polystyrene latex," Phys. Rev. A **42**, 7347–7354 (1990).
17. K. Goyal, M. Dong, V. Nguemaha, B. Worth, P. Judge, W. Calhoun, L. Bali, and S. Bali, "Empirical model of total internal reflection from highly turbid media," Opt. Lett. **38**, 4888–4891 (2013).
18. See, for instance, S. Mariani and M. Minunni, "Surface plasmon resonance applications in clinical analysis," Anal. Bioanal. Chem. **406**, 2303–2323 (2014).
19. W. Calhoun, H. Maeta, A. Combs, L. Bali, and S. Bali, "Measurement of refractive index of highly turbid media," Opt. Lett. **35**, 1224–1226 (2010).
20. W. Calhoun, H. Maeta, A. Combs, L. Bali, and S. Bali, Reply to Comment on "Measurement of refractive index of highly turbid media," Opt. Lett. **36**, 3172 (2011).
21. M. Dong, K. Goyal, B. Worth, S. Makkar, W. Calhoun, L. Bali, and S. Bali, "Accurate *in situ* measurement of complex refractive index and particle size in intralipid emulsions," J. Biomed. Opt. **18**, 087003 (2013).
22. See, for example, Fig. 1 in M. Kyrish, U. Utzinger, M. R. Descour, B. K. Baggett, and T. S. Tkaczyk, "Ultra-slim plastic endomicroscope objective for non-linear microscopy," Opt. Express **19**, 7603–7615 (2011), The absorption coefficient in the visible wavelength range (400–700 nm) is ≤0.2/cm, which is negligible compared to the α-values arising primarily from scattering that are considered in our work.
23. M. Broide and R. Cohen, "Measurements of cluster-size distributions arising in salt-induced aggregation of polystyrene microspheres," J. Colloid Interface Sci. **153**, 493–508 (1992).
24. M. McClimans, C. LaPlante, D. Bonner, and S. Bali, "Real-time differential refractometry without interferometry at a sensitivity level of 10^{-6}," Appl. Opt. **45**, 6477–6486 (2006).
25. V. Kontturi, P. Turunen, J. Uozumi, and K. Peiponen, "Robust sensor for turbidity measurement from light scattering and absorbing liquids," Opt. Lett. **34**, 3743–3745 (2009), and references therein.
26. O. Vázquez-Estrada and A. García-Valenzuela, "Optical reflectivity of a disordered monolayer of highly scattering particles: coherent scattering model versus experiment," J. Opt. Soc. Am. A **31**, 745–754 (2014).
27. E. Gutiérrez-Reyes, A. García-Valenzuela, and R. G. Barrera, "Extension of Fresnel's formulas for turbid colloidal suspensions: A rigorous treatment," J. Phys. Chem. B **118**, 6015–6031 (2014).
28. J. Räty, I. Niskanen, and K.-E. Peiponen, "Fresnel reflectance in refractive index estimation of light scattering solid particles in immersion liquid," Appl. Phys. Lett. **96**, 231112 (2010).
29. D. Huh, J. Bahng, Y. Ling, H. Wei, O. Kripfgans, J. Fowlkes, J. Grotberg, and S. Takayama, "A gravity-driven microfluidic particle sorting device with hydrodynamic separation amplification," Anal. Chem. **79**, 1369–1376 (2007).
30. This estimate corrects a typographical error in Ref. [17].

31. See, for example, Y. Liu and P. H. Daum, "Relationship of refractive index to mass density and self-consistency of mixing rules for multicomponent mixtures like ambient aerosols," Aerosol Sci. **39**, 974–986 (2008).
32. See, for example, A. Zangwill, *Modern Electrodynamics* (Cambridge University, 2012), Fig. 21.9, p. 788.
33. X. Ma, J. Lu, R. Brock, K. Jacobs, P. Yang, and X. Hu, "Determination of complex refractive index of polystyrene microspheres from 370 to 1610 nm," Phys. Med. Biol. **48**, 4165–4172 (2003).
34. A. H. Contreras-Tello and A. García-Valenzuela, "Refractive index measurement of turbid media by transmission of backscattered light near the critical angle," Appl. Opt. **53**, 4768–4778 (2014).
35. B. K. Siesjö, "Acid-base homeostasis in the brain: hysiology, chemistry, and neurochemical pathology," Prog. Brain Res. **63**, 121–154 (1985).
36. H. Kazemi and D. C. Johnson, "Regulation of cerebrospinal fluid acid-base balance," Physiol. Rev. **66**, 953–1037 (1986).